RSC Advances

ROYAL SOCIETY OF CHEMISTRY

www.rsc.org/advances

Modeling of polystyrenic nanoparticles driven β-trans-crystalline efficiency in isotactic polypropylene

S. Habibpour, J. Zabihirad, N. Mohammadi* and H. Mohammadi

Nano and Smart Polymers Center of Excellence, Department of Polymer Engineering and Color Technology, Amirkabir University of Technology, P.O. Box 15875-4413, Tehran, Iran
Loghman Fundamental/Technological Research Group, P.O. Box 15875-4413, Tehran, Iran

Abstract

Addition of 2 wt.% mono-size, 180 nm in diameter, soft nanoparticles (SNPs) of linear and cross-linked polystyrene (PS and XPS) and styrene-acrylonitrile copolymers containing 25 wt.% acrylonitrile (SAN25 and XSAN25) induced relative β-polymorphism as much as 20, 27, 34 and 10% during 10 minutes annealing of isotactic polypropylene (iPP) at 116 °C, respectively. It became nil, however, by changing the annealing conditions: time and/or temperature. The β nucleation efficiency of the studied SNPs were modeled based on their normalized phenyl groups surface accessibility to the methyl groups of matrix chains profusion divided by the main components commensuration mismatch multiplied or divided by absolute particle rigidity at the crystallization conditions. A bi-exponential function with four constants could be fitted over the extracted data points rationalizing the kinetic and thermodynamic aspects of the phenomenon.

Keywords: Polypropylene, β nucleating agent, Soft styrenic nanoparticles, phenyl d-spacing.

Introduction

Tuning the crystal structure of semi-crystalline polymers is considered a long standing significant issue mainly affecting their physical and mechanical properties. Among diverse synthetic and biological semi-crystalline polymers, iPP shows at least four polymorphisms: α, β, γ, and smectic with unique chain conformation of 3_1 helices. α-iPP with monoclinic unit cell is the most common modification. β-polymorphism of iPP, however, is hexagonal, while orthorhombic unit cell forms γ modification. Finally, smectic iPP implies chain orientation somewhere between its ordered and amorphous phases. β and γ modifications are induced through temperature gradient, application of flow fields and specific nucleating agents [1–6]. The β implementation has been started since 1990's [7,8] and the enhanced mechanical properties were

assigned to probable β-α crystal transition through thermo/mechanical motives. In other words, the instability of β nucleated iPP was assigned to its thermodynamic characteristics resulted in structural transition during the course of annealing or mechanical loading leading to enhanced permeability and toughness. Addition of suitable nucleating agents to iPP was introduced as the most efficient approach for increasing its β modifications resulting in enhanced toughness [8–11]. They are classified as aromatic ring containing compounds and selective metal salts of group IIA and their di-carboxylic acids. γ-quinacridone and calcium salt of imido acids, calcium stearate and pimelic acid can be mentioned as few examples for groups one and two, respectively. Recently, β-iPP was prepared through selective benzene ring containing synthetic polymers such as PS, SAN and poly(styrene-co-butadiene) rubber (SBR) [6,12–14]. In addition to their easy processing, they are cheaper than common β-nucleators, while relaxing some of their side hazards [6]. The extended dimensional lattice matching or epitaxial growth has been proposed as plausible theory for rationalizing the involved structural evolutions [6]. Scrutinizing the nucleation mechanisms depicted the critical role that microstructure and chain conformation played during the course of crystallization process [15]. Heterogeneous nucleation resulted in enhanced surface-induced crystallization rate depending on film thickness, temperature and the inter-molecular interactions affecting crystal structure and morphology. Epitaxial matching among the matrix polymer chain and the surface of nucleating agent, however, is the main effective mechanism of polymorphism control [16]. Fundamentally speaking, polymorphism can be induced by even amorphous polymers provided that they can initiate surface matched epitaxial growth through providing appropriate physical aspects namely residual order, interfacial energy, roughness and physical state [13,16–19]. For example, polystyrenics carrying benzene ring could induce β modification in iPP through nucleation with suitable d-spacing [12]. The residual order, however, is affected by co-monomer type, extent of cross-linking and material state at crystallization conditions: glassy or rubbery [20]. The conformational modification of isotactic PS (iPS) during crystallization and its phenyl groups surface accessibility and orientation were also introduced as other motives regarding epitaxial matching of isotactic polystyrene/isotactic polypropylene (iPS/iPP) [12,21,22]. Accordingly, thermal history and resultant β crystal content represented two major parameters affecting recrystallization [4,23].

The main goal of current research has been to develop a better understanding regarding β nucleation in iPP using styrenic nanoparticles. The efficiency of β modification were modeled

based on the physical state of nanoparticles during crystallization, their phenyl groups surface accessibility and the matrix chains/particles d-spacing mismatch. The physical rational was then changed into a phenomenological bi-exponential model with four constants based on the spirits of Hoffman's nucleation theory.

Experimental

Materials A fiber grade iPP with melt flow index of 3 g/10 min (230 °C and 2.16 kg) was purchased from Arak Petrochemical Co. Styrene (St) and acrylonitrile (AN) monomers, sodium lauryl sulfate (SLS, ionic surfactant), triton X-100 (nonionic surfactant), potassium persulfate (KPS, initiator), tert-Dodecylmercaptan (TDM, chain transfer agent), potassium hydroxide (KOH, pH regulator), divinyl benzene (DVB, cross linker), dimethylformamide (DMF), toluene and xylene were supplied from Merck. Double distilled water (DDW) and methanol were purchased from Kimidaroo and Dr. Mojalali of Iran, respectively.

Emulsion polymerization Mono size nanoparticles of PS, XPS, 25 wt. % acrylonitrile containing SAN25 and XSAN25 with particle size of 180 nm were synthesized by emulsion polymerization in tumbling reactor at 60 °C for 24 h based on pre-designed recipes [24], Table 1. The ingredients were thoroughly mixed and added to 115 cm^3 glass bottles with filing factor of 87 %. The conversion of each polymerization process was determined almost 100% by gravimetric technique. Ionic and nonionic surfactants of the synthetized soft nanoparticles were removed in three steps with 60 °C water and methanol, respectively [24].

Table 1 Emulsion polymerization recipes

Materials	PS400 (g)	XPS (g)	SAN25-500 (g)	SAN25-200 (g)	SAN25-70 (g)	SAN50-500 (g)	XSAN25 (g)
St	10	8	7.5	7.5	7.5	5	7.5
AN	0	0	2.5	2.5	2.5	5	2.5
DVB	0	2	0	0	0	0	2.4
DDW	90	90	90	90	90	90	90
KPS	0.05	0.05	0.05	0.05	0.05	0.05	0.05
SLS	0.015	0.015	0.015	0.015	0.015	0.015	0.015
Triton X-100	0.3	0.3	0.3	0.3	0.3	0.3	0.3
KOH	0.015	0.015	0.015	0.015	0.015	0.015	0.015
TDM	0	0	0	0.025	0.04	0	0

Particle characterization The size and size distribution of synthesized latex particles were determined by Mastersizer 2000, Malvern dynamic light scattering (DLS).

Viscosity average molecular weight Average molecular weights of iPP, PS and SAN were determined via dilute solution viscometry using Mark-Houwink-Sakurada (MHS) constants in 85 °C xylene and 30 °C toluene and dimethylformamide, respectively [25].

Film preparation and thermal annealing iPP and 2 wt. % of each SNP were blended in internal mixer, Brabender Co., at 190 °C and 60 rpm for 10 minutes. Films, 70 or 500 μm in thickness were pressed at 200 °C and 80 atmospheres between Tin plates (500 μm in thickness) and air cooled. The films were then annealed at 105, 116 and 126 °C and immediately cooled to room temperature.

Differential scanning calorimetry The glass transition, crystallization and melting peaks were measured via heating and immediate cooling of samples from −20 to 210 °C at 10 °C/min ramp with an indium calibrated Perkin-Elmer Pyris1 under 80 ml/min nitrogen purging. The sample crystalline content was calculated by melting enthalpy divided by the intrinsic enthalpy of perfect crystal (ΔH_{id}° = 177 J/g).

Optical Microscopy The crystal morphology was assessed on 70 μm thick films with hot stage equipped cross-polarized optical microscope (POM), Carl Zeiss Jena (Jenapol).

Scanning Electron Microscopy Dispersion of soft nanoparticles within iPP was evaluated with surface analysis of fractured films in liquid nitrogen. The cross-section of each film was coated with a thin layer of gold before its examining by SEM, AIS2100 model of Seron Technology instrument. The magnification was 10 K.

Wide Angle X-ray Diffraction An Inel Equinox 3000 (Germany) instrument with Cu-Kα radiation with λ= 0.154 nm at 2θ= 5-35° was used. Experiments were done in reflection mode using a disc type detector. The principal reflections of the α-crystals are (110) at 2θ= 14.1°, (040) at 16.9°, (130) at 18.5°, while (300) at about 15.9° implies the principal reflection of β-crystal form [2]. Consequently, the relative percentage of β-polymorphism was calculated from curve fitting on XRD graphs and reflection peaks using a Gaussian function.

$$K_{\beta} = \frac{A_{\beta(300)}}{A_{\alpha(110)} + A_{\alpha(040)} + A_{\alpha(130)} + A_{\beta(300)}} \quad (1)$$

Results

Figure 1a shows the population of synthesized particles in volume percent versus their sizes for SAN25-500 latex. The average particle size of SAN25-500 was estimated to be 180 nm while its size distribution index was equal to 1.06. The SEM image of the dried SAN25-500 particles was shown in Figure 1b.

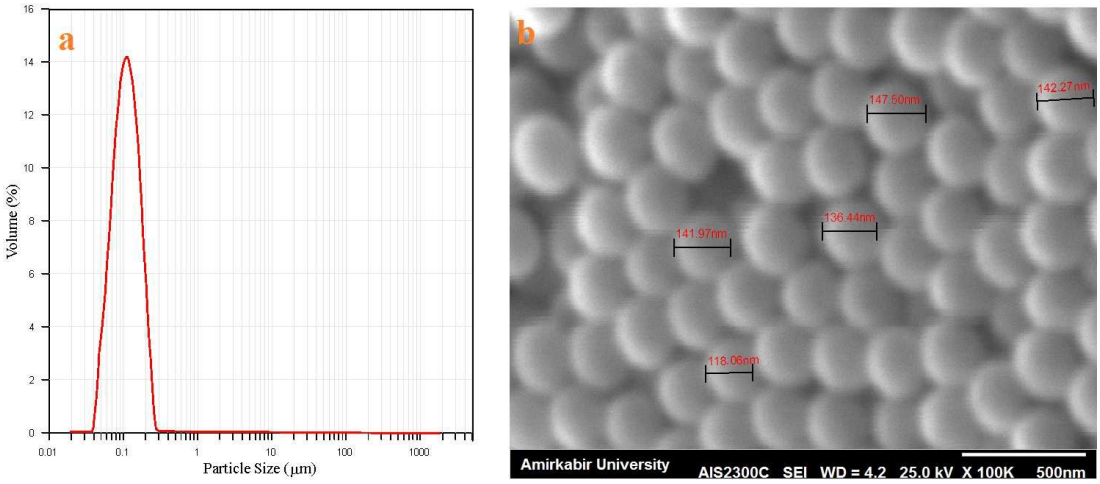

Fig 1 Population of SAN25-500 particles in volume percent versus particle size (a) and SEM image of the dried particles (b)

Molecular characteristics of the iPP and synthesized linear and cross-linked nanoparticles were tabulated in Table 2.

Table 2 Molecular characteristics of the iPP and synthesized linear and cross-linked nanoparticles

Materials	% Acrylonitrile	M_v (kg/mol)	Tg (°C)	Tm (°C)	K_H	MHS constants
PP	-	168	2.7	167.5	0.48	A = 0.63, k = 0.096 ml/g
PS	-	400	102	-	0.18	A = 0.72, k = 0.0092 ml/g
XPS	-	-	126	-	-	-
SAN25-500	25	500	102	-	0.23	A = 0.71, k = 0.0012 ml/g
SAN25-200	25	200	-	-	-	"
SAN25-70	25	70	-	-	-	"
SAN50-500	50	500	102	-	-	"
XSAN25	25	-	120		-	-

The phase diagrams of SAN or PS blends with the iPP were calculated based on the Mayes's model, Figure 2 [26,27]. All samples showed upper critical solution temperature (UCST) with spinodals at 7500, 5800, 3900, 8100 and 8500 K for 2 wt. % filled iPP with SAN25-500, SAN25-200, SAN25-70, SAN50-500 and PS400, respectively.

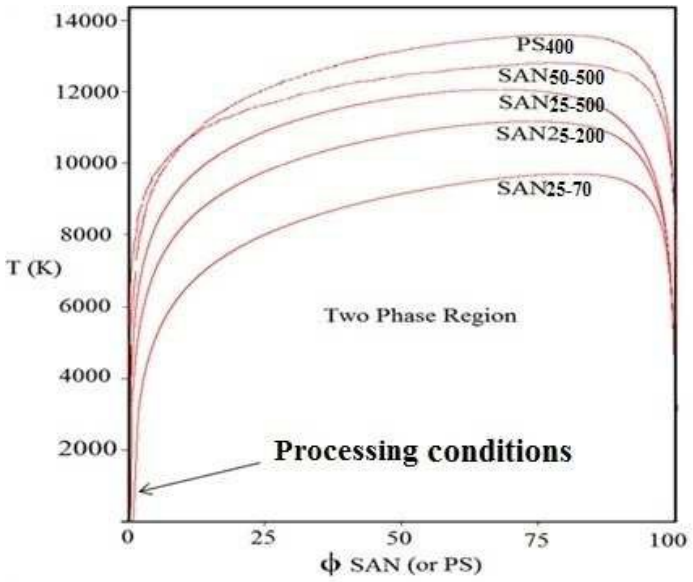

Fig 2 The phase diagrams of filled iPP with linear SANs and PS400 at atmospheric pressure

The SEM images of iPP and filled iPPs with 2 wt. % SAN25-500 and XPS depicted size distributions somewhere between 180-900 nm and 200 nm, respectively, Figure 3.

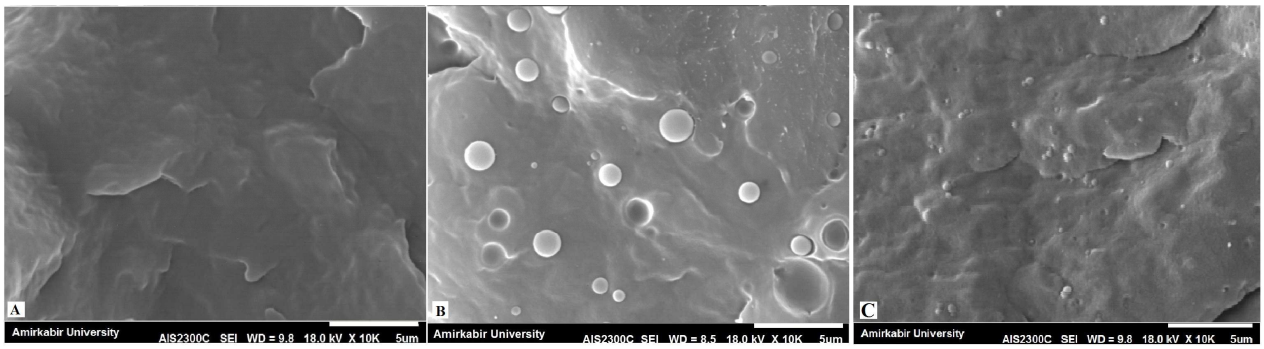

Fig 3 SEM images of A) iPP, B) iPP/SAN25-500, and C) iPP/XPS

The cross polarized optical images of iPP containing 2 wt. % PS400, SAN25-500, SAN25-200 and SAN25-70 showed brighter β crystals than α one, Figures 4 A-D.

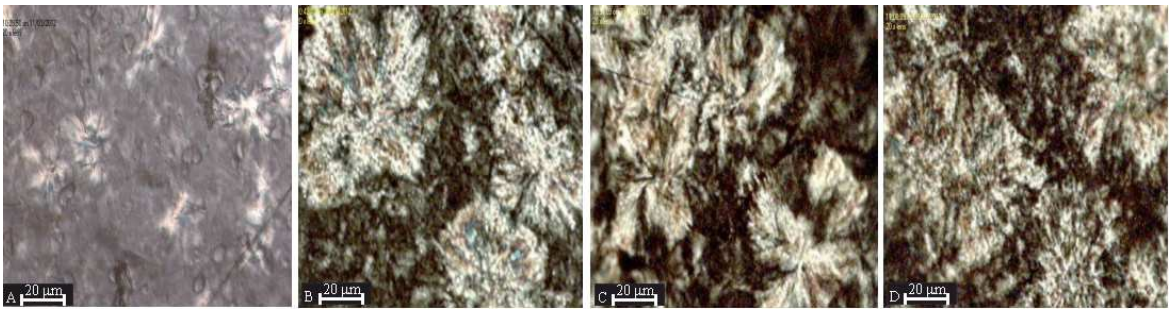

Fig 4 Cross-polarized optical microscope images of filled iPP with: (A) PS400, (B) SAN25-500, (C) SAN25-200 and (D) SAN25-70, scale bar depicts 20µm.

Distinct melting temperatures and polymorph evolutions were also determined from POM images, Figure 5. The melting of β crystals started at temperatures lower than 149 °C and completed at 151 °C. Its re-crystallization to α-polymorph, however, initiated at temperatures lower than 156 °C and then all crystallites melted at 166 °C.

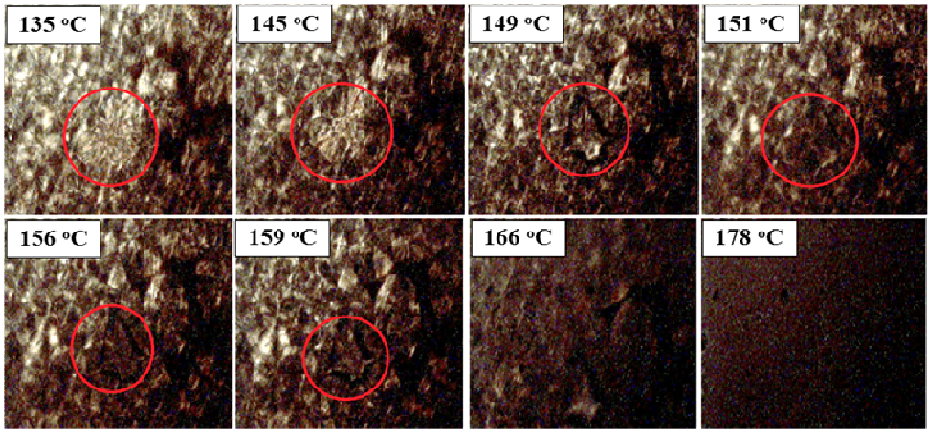

Fig 5 Cross-polarized optical microscopy of 2h annealed iPP/SAN25-500 during heating by 10 C min^{-1}

The intra-molecular rearrangements of linear and cross-linked nanoparticles were analyzed using thermal annealing hysteresis, Figure 6. As one can observe, the glass transitions of both samples shifted to lower temperature during the cooling run with respect to heating run, while the linear SAN25-500 showed more sensible relaxation at glass transition.

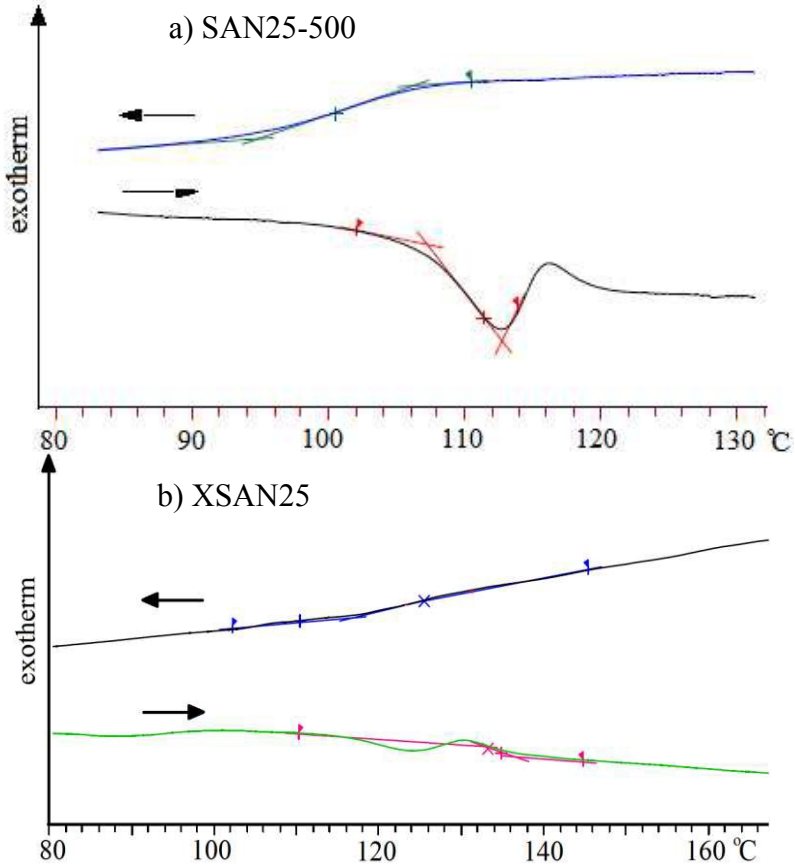

Fig 6 DSC Heating and cooling runs regarding a) SAN25-500 and b) XSAN25 in

XRD graphs of iPP films containing different SNPs were shown in Figure 7. Isothermal crystallization of filled iPP with SAN25-500, XPS, PS400 and XSAN25 at 116 °C for 10 minutes led to 34, 27, 20 and 10 percent of relative β-polymorph, respectively, Figures 7a-d.

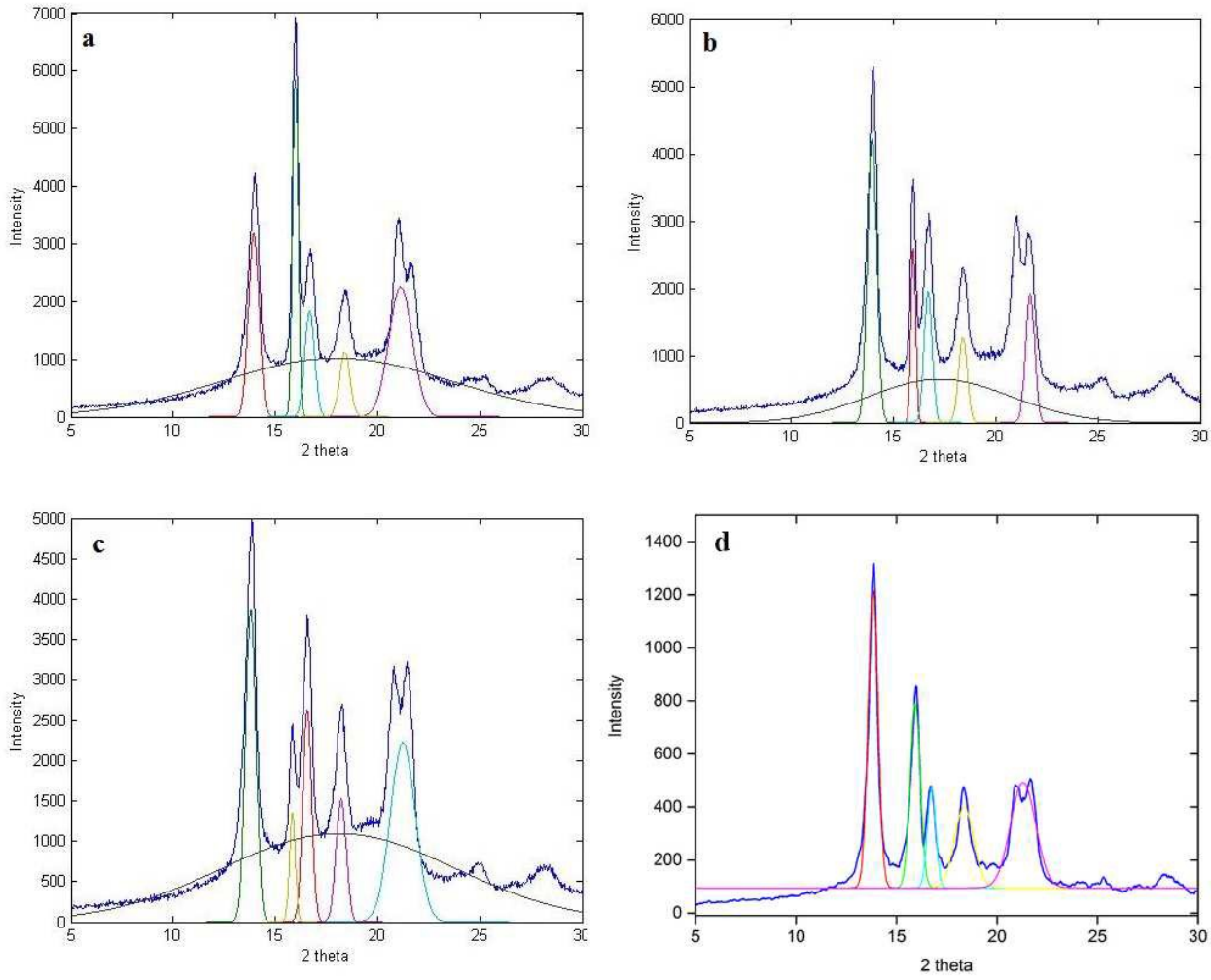

Fig 7 XRD graphs of iPP nano-composites: (a) SAN25-500, (b) PS400, (c) XSAN25 and (d) XPS at 116 °C for 10 minutes.

Crystallization time increase to 2h reduced the relative β modification of iPP/SAN25-500 to 10%, Figure 8a. Two hours annealing at 105 and 126 °C, however, did not lead to any β-polymorph at all, Figure 8b,c. Crystal content and relative β-polymorphism (K_β) of all analyzed samples were collected in Table 3.

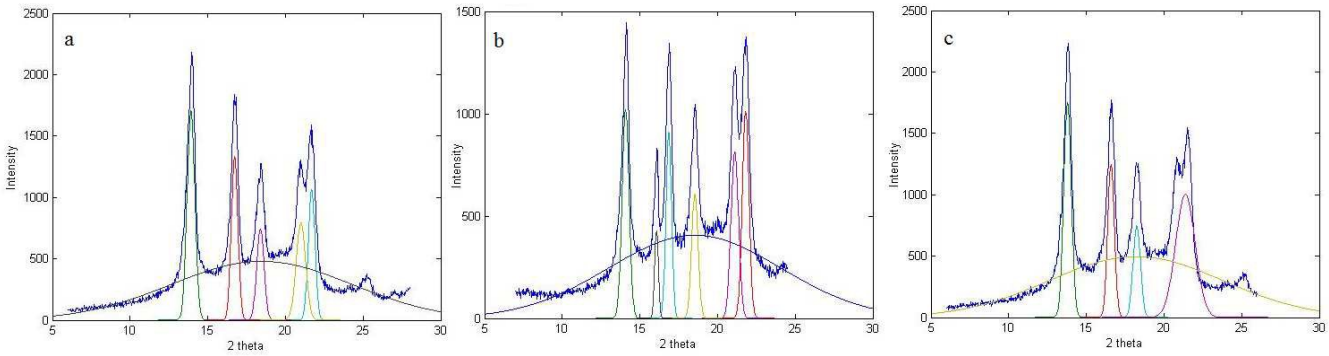

Fig 8 XRD graphs of iPP nano-composites containing SAN25-500 at (a) 105°C (b) 116°C and (c) 126°C for 2 hours

Table 3 Physical and thermo-mechanical characteristics of neat and filled iPPs

Sample	Annealing time (min)	Crystal content (%)	K_β %	T_c (°C)	T_m (°C)
iPP	120	49.3	0	110.3	167
iPP/PS400	10	49	20	115.6	
iPP/PS400	20	51	9.5		
iPP/SAN25-500	10	49	34	115.2	
iPP/SAN25-500	20	50	16		165.8
iPP/SAN25-500	120	49	10		165.4
iPP/SAN25-500	600		6.2		
iPP/XSAN25	10		10	113.2	
iPP/XSAN25	20		5		

The effect of crystallization time on the relative β-polymorph of filled iPP containing SAN25-500 at 116 °C was depicted in Figure 9. The nucleation efficiency was enhanced by crystallization time, maximized at 10 minutes and diminished to negligible magnitude later on. Quenched melt of iPP/SAN25-500 to room temperature, its annealed version at 116 °C for 24 h followed by quenching into room temperature also did not show any β-polymorph.

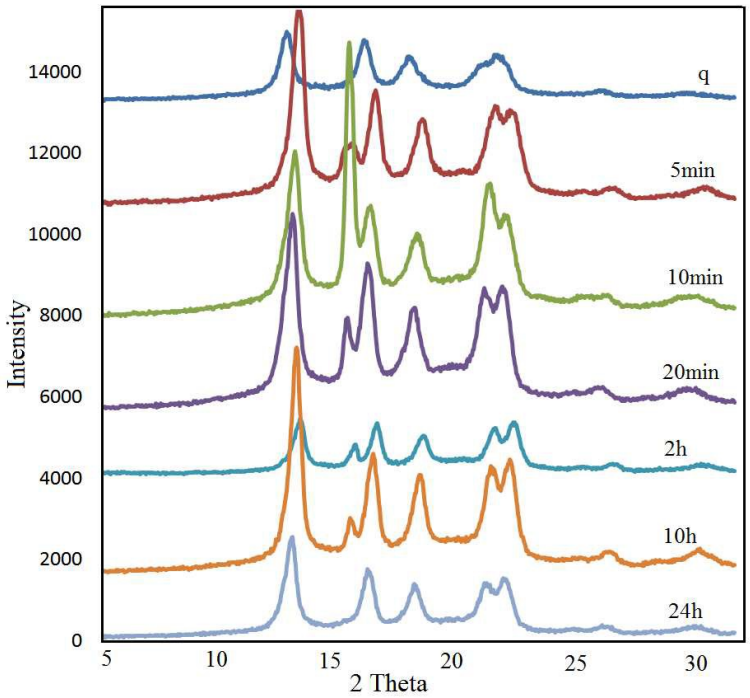

Fig 9 XRD graphs of crystallized filled iPP containing 2 wt% of SAN25-500 at 116 °C versus time

Discussion

Molecular weight decrease of SAN25 from 500 to 70 kg/mol reduced the spinodal temperature from 7500 to 3500 K in its 2 wt. % blend with iPP. However, it was raised back to 8100 K by its acrylonitrile content increase to 50 percent (SAN50-500). PS chains, 400 kg/mol in molecular weight, however, showed the maximum spinodal in blend with iPP. Nonetheless, there was no significant difference among POM images or relative β modifications (K_β) of the filled iPP with different molecular weight SAN or PS400 particles, Figure 4 A-D. In other words, the effect of polystyrenic molecular weight on the nucleation event, and phase evolution were nil. The nucleation event was located in two phase regions in all studied cases starting from the melt and continued down into the semi-crystalline iPP containing glassy SNPs, Figure 2. Therefore, only the results of the filled iPP with 2 wt. % SAN25-500 will be reported. Dispersion average size of SAN25-500 and XPS nanoparticles in the iPP appeared in the range of 180-900 nm and 180 nm, respectively, Figure 3B and C. The nanoparticles showed strong tendency to agglomeration due to their high interfacial tension with iPP. Accordingly, it led to Oswald ripening of particles containing linear copolymers in the processing conditions, Figure 3B. The surface area decrease through Oswald ripening resulted in reduced β crystal formation efficiency. Cross-linked particles, however, forbid nanoparticles inter-diffusion leaving them in original size, Figure 3C.

The growth rate of β-polymorphism in the range of 105-140 °C is higher than α modification in iPP [6,10,15,28]. Temperature rise enhances β-polymorphism probability thermodynamically; while its lower melting temperature with respect to α crystal declines its formation statistics kinetically. Accordingly, isothermal crystallization of iPP/SAN25-500 at 126 °C and 105 °C, both showed reduced relative β-polymorphism with respect to crystallization at 116 °C, Figure 8a,c. Maximum β modification was discernible at 10 minutes of thermal annealing at 116 °C, Figure 10. Longer and shorter annealing also declined the relative β-polymorph of the iPP containing SAN25-500, PS400 and XSAN25. The total crystallization time of iPP at different annealing temperatures was reported 5 to 20 minutes [29]. Long time annealing increased the thickness and lateral sizes of nucleated lamella through re-crystallization, polymorphic phase transition and limited molecular rearrangement in the amorphous phase resulting in crystal perfection [30]. Accordingly, time resolved evolution of unstable β-polymorph into α type can be noticed, Figure 5. In addition, melting behavior of β-polymorph depends mainly on sample thermal history. β to α evolution via annealing after non-isothermal crystallization and cooling to room temperature was also reported [31]. Annealing after cooling to temperatures higher than 100 °C, did not show any α transformation. It was attributed to partial and fragmented α crystal formation within β phase amplifying secondary crystallization [10].

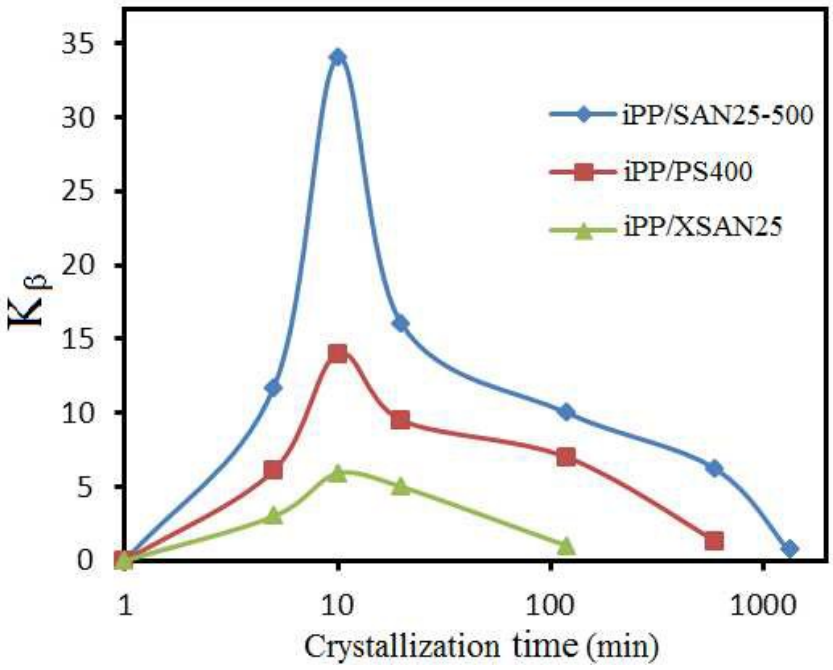

Fig 10 Effect of crystallization time on the relative β modification (K_β) of filled iPP containing SAN25-500, XSAN25 and PS400

Annealing also caused β phase to α transition along with local melting of its crystal mixture acting as α nucleating agents. Isothermal crystallization of random iPP copolymers with small amount of co-monomer enhanced β-α transition at all temperatures due to higher crystallization rate of the former [6]. Furthermore, surface recrystallization on lamella through perfection or thickening of β-polymorph led to more stable α form with higher melting temperature [6]. Therefore, long time annealing resembles temperature increase activating β-α transition resulting in reduced relative β content.

The type, size and nature of mobile and immobile amorphous fractions of semi-crystalline polymers are also affected by the crystallization temperature. The observed decrease and increase of temperature transitions regarding β and α polymorphs, respectively, was assigned to loose and mobile amorphous fraction of the former and higher oriented length of the latter [30]. A saturation time of 10 minutes was reported regarding the orientated iPP with β-polymorph as relatively short annealing time.

In addition to crystallization time, the acrylonitrile content and cross-linking of SNP may affect its β nucleation efficiency in iPP. SAN could nucleate epitaxial crystals in iPP via furnishing surfaces with the required characteristics. The dimensions of orthorhombic unit cell of polyacrylonitrile are 21.18, 11.6 and 5.1 Å in a, b and c axis, respectively [32]. The intermediate dimension is close to the β-polymorph of iPP and calcium dicarboxylate [33]. Copolymerization with styrene, however, not only reduces -C≡N groups interactions among, but also causes mobility rise and constitute regularity forbidding inter chain crystallization. Accordingly, SAN25-500 particles did not show any characteristic XRD crystalline peak regarding PAN (2θ = 16.8 or d-spacing = 2.6 Å [35]), Figure 11. However, no crystallization was detected in copolymers containing more than 50 wt. % styrene [34].

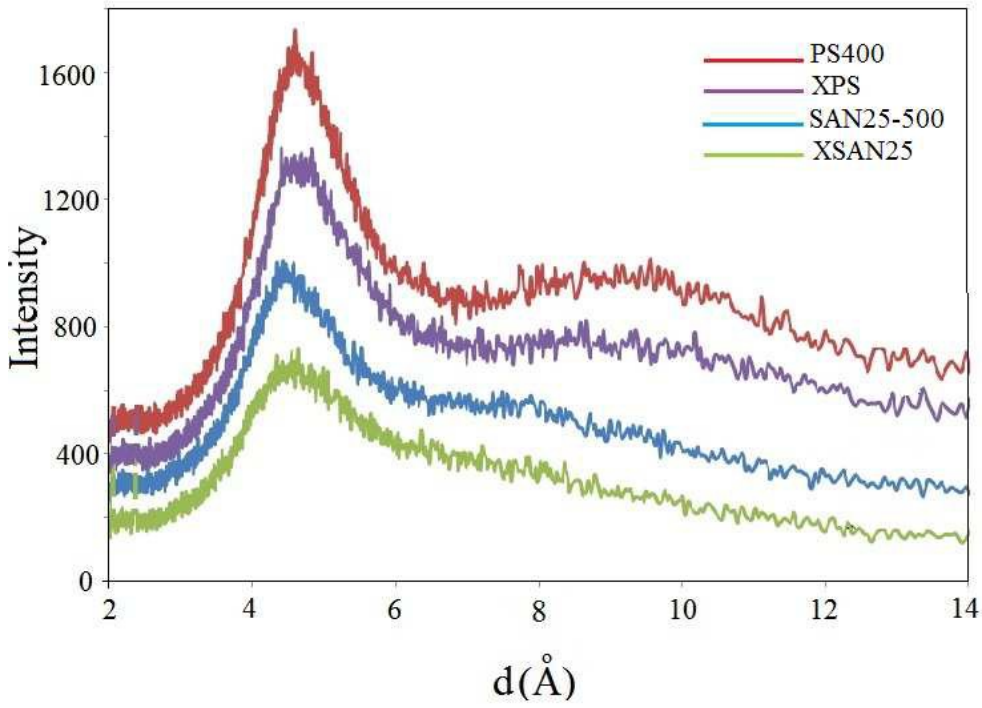

Fig 11 XRD graphs of SAN25-500, XSAN25, PS400 and XPS nanoparticles

Su et al.[6], assigned the high β-polymorph and nucleation efficiency with SAN filled iPP (with 23 wt% of acrylonitrile) to structure change due to polar groups rather than PS contribution. The interactions among methyl groups of iPP/phenyl groups of iPS previously proposed as the main controlling parameter affecting α or β nucleation [12]. Unit cell dimensions of hexagonal crystals containing 3_1 helix chain of iPS are a = b = 21.9 Å and c = 6.65 Å. Therefore, micro-segregation of phenyl groups may form ordered stacks with d-spacing of 6.65 Å. Phenyl stacks with periodicity lower than 5 Å in amorphous PS also represents its local isotactic habit via expanded phenyl group interactions. Therefore, stacked phenyl groups sometimes form local order [36]. Phenyl stacking with d-spacing of either crystalline or amorphous iPS can behave as versatile nucleating agents of iPP, 6.6 Å as β modifier and 5 Å as α modifier [12]. In addition, β-polymorph formation in iPP using atactic PS (aPS) was already reported [13]. Higher nucleation efficiency of SAN25-500 and XPS with respect to PS400 and XSAN25 can be attributed to the chain conformational transitions with local orders acting as nucleating particles complemented with the SNPs state at the crystallization temperature.

WAXS analysis of aPS, iPS and its comparison with styrene confirmed the peaks at d = 8.38 Å and d = 10.13 Å for the polymers representing styrene polymerization [36]. In other words, the

second peak of XRD graph of styrenic SNPs, on the highest d-spacing, assigned as the polymerization peak [36–38]. The synthetized particles showed similar peaks at 8.9, 8.8, 7 and 7.1 Å for PS400, XPS, SAN25-500 and XSAN25, respectively, Figure 11. The intense peak at d-spacing of 4.5 Å was attributed to at least two different types of interatomic spacing: those between atoms in alternate phenyl groups of the same chain and those between phenyl groups and neighboring chain atoms, forming stacked phenyl group nearby the surface of SNPs [36–38]. Nonetheless, different surface and bulk oriented stacks of styrene phenyl rings is feasible looking at the synthesized particles [21,22]. The surface segregation of phenyl groups along c axis of phenyl ring of aPS (the vector between backbone carbon atoms and para-position carbons) reported normal to the surface [21]. Empirical measurement of the layered structures of PS at the air interface and different solids, also proved phenyl rings stacking and a curvature with angle of 20° and 35° with respect to the normal of surface, respectively [22,39]. It was also shown that the phenyl groups stacking at the surface of free films is toward outside [40].

Consequently, epitaxiallity was assigned to dense stacking of phenyl groups at the surface of SNPs during iPP crystallization, Figure 12.

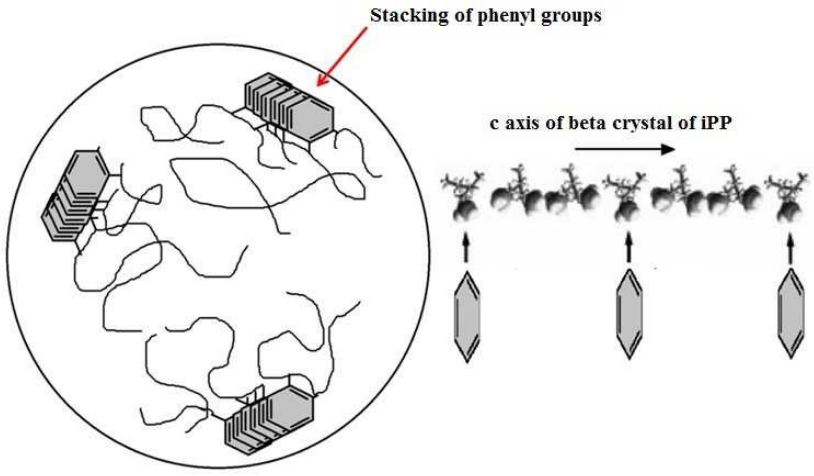

Fig 12 Intra stacking of phenyl groups in PS and SAN (left) and Phenyl group matching with periodicity in c-axis β-iPP crystallite (right)

Therefore, the d-spacing effect of dense phenyl groups on matrix chain orientation during crystallization, with approximate characteristic dimension of c axis of β-iPP was proposed as the main origin of β-polymorph formation, Figure 12. Phenyl groups d-spacing of PS400 and XSAN25 or XPS SNPs were lower and higher than SAN25-500, respectively. Accordingly, the relative β crystalline content of iPP was the highest for SAN25-500. Thus, epitaxial matching

between the stacked phenyl groups of nucleating particles, β crystalline unit cell dimension of iPP and the surface accessibility of the former for van der Waals interactions with methyl groups of iPP were nominated as the effective key players besides the state of SNPs at the crystallization conditions. The surface energy difference among SNPs and the matrix may also assign with finite role as another effective parameter regarding the nucleation efficiency.

Consequently, β nucleation efficiency of SNPs consists the normalized disparity between the phenyl ring d-spacing (d_{ph}) and the β-polymorph dimension of iPP (d_{β}) by the latter, relative intensity of stacked phenyl groups at the surface of particles, (I_{rel}), and the structural rigidity of particles (the absolute crystallization temperature minus the glass transition temperature of β nucleator). The stacked phenyl groups normalization characteristic was the polymerization peak intensity:

$$d_{dif} = \frac{d_{ph} - d_{\beta}}{d_{\beta}} \quad (2)$$

$$I_{rel} = \frac{I_{ph}}{I_{polym}} \quad (3)$$

$$A = |T_c - T_g| \quad (4)$$

Here, d_{ph} is average phenyl rings d-spacing of particles, while d_{β} is the characteristic of β-polymorph of iPP (6.6Å). I_{ph} is the peak intensity of stacked phenyl groups, while I_{polym} is polymerization peak in XRD curves of the synthesized nanoparticles, Figure 11. The parameters were calculated using XRD data regarding the synthesized nanoparticles, Figure 11, and tabulated, Table 4.

Table 4 Characteristics of polystyrenic soft nanoparticle

Sample	K_{β}	d_{ph}	d_{dif}	I_{ph}	I_{poly}	I_{rel}	A	$I_{rel}*A/d_{dif}$ or $I_{rel}/d_{dif}*A$
XSAN25	10	4.858	0.252	536.746	202.135	2.655	4	42.046
PS400	20	4.539	0.301	1087.11	339.223	3.204	14	1.318
XPS	27	4.789	0.263	877.954	304.709	2.881	10	109.458
SAN25-500	34	4.452	0.315	703.746	251.773	2.795	14	0.633
Phillips et al. [12]	26	4.43	0.318	4921.05	3236.84	1.520	10	0.477

β nucleation efficiency decreased by $(d_{ph} - d_{\beta})$ increase or enhanced mismatching. The stacked phenyl groups intensity rise amplified β nucleation efficiency, while the absolute characteristic temperature difference (A) could increase or decrease the relative percent of β-polymorph. So, $I_{rel} \times A(d_{dif})^{-1}$ or $I_{rel}(d_{dif} \times A)^{-1}$ were the controlling variables of nucleation efficiency regarding the studied SNPs, Figure 13. Growth rate of α modification and Hoffman's nucleation theory were considered as the basis of correlating the K_{β} to the nucleation efficiency (X):

$$K_{\beta} = a\exp(bX) + c\exp(dX) \tag{5}$$

Where

$$\begin{cases} X = \dfrac{I_{rel} \times (T_g - T_c)}{d_{dif}} \xrightarrow{if} T_g > T_c \\ X = \dfrac{I_{rel}}{d_{dif} \times (T_g - T_c)} \xrightarrow{if} T_g < T_c \end{cases}$$

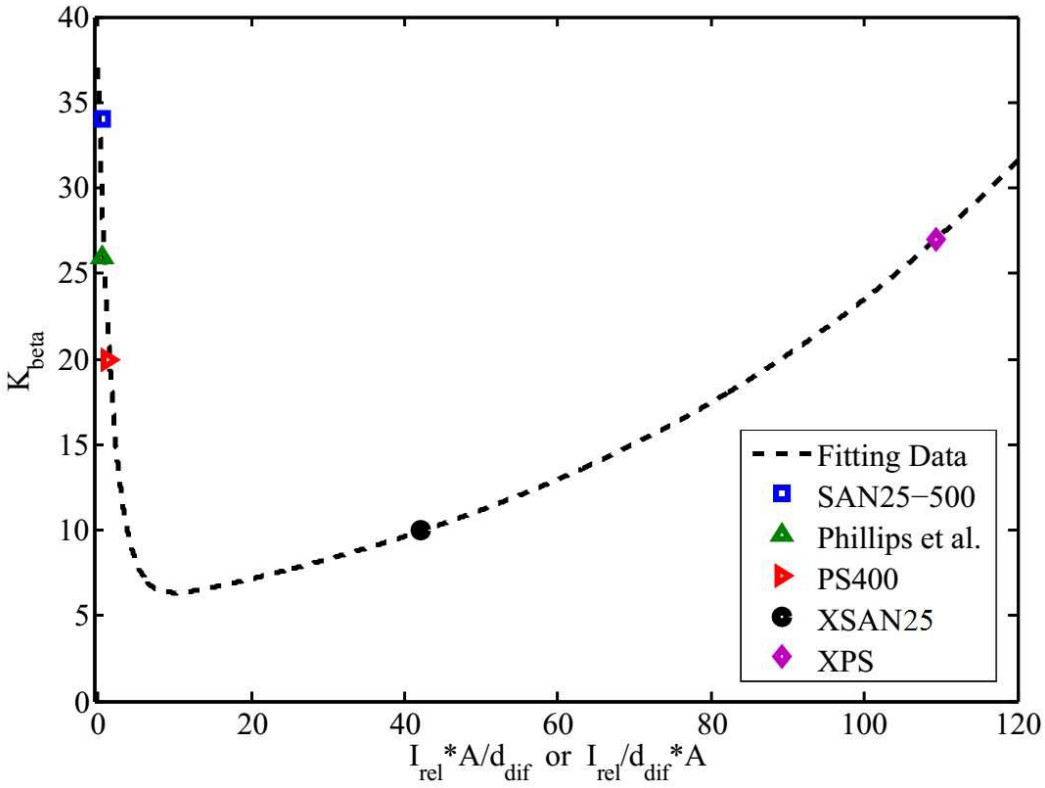

Fig 13 K_{β} of SNPs versus average phenyl d-spacing, their stacks accessibility to the crystallizing chains and structural rigidity of SNPs

The coefficients of a, b, c and d were found 31.7, -0.51, 5.3 and 0.01, respectively. The nucleation efficiency of β-polymorphism declined by substituting PS400 instead of SAN25-500 and then increased by XSAN25 and XPS. Nanoparticles glass transition increase by simultaneous cross-linking and copolymerization over crystallization temperature, 116 °C, played a major role in nucleation efficiency. On the other hand, the formation of crystal nucleus can be magnified by relative immobility or chain rigidity at crystallization temperature. Soften nanoparticles by approaching T_gs led to their enhanced entropy resulting in surface rearrangements with reduced β-polymorph efficiency and vice versa. The minimum β crystal efficiency was achieved by approaching the SNPs glass transition with spatially heterogeneous dynamic locating at the minimum of the presented model, Figure 13.

Despite the minute d-spacing difference between SAN25-500 and XSAN25, their β nucleation efficiency were quite different, Table 4. It can be attributed to their chains dynamic disparity at crystallization conditions due to XSAN25's networking, Figure 6. XSAN25 could be deficient in phenyl ring stacks diminishing surface segregation based nucleation. The nucleation efficiency decrease using XSAN25 complemented its reduced β-polymorph efficiency in comparison to SAN25-500 in the iPP crystallization. On the other hand, d-spacing disparity and resultant crystallizing chains mismatched with surface segregated phenyl ring stacking in PS400 reduced its β-polymorph efficiency. The hydrophilic character of acrylonitrile (AN) monomer in emulsion copolymerized SAN may cause acrylonitrile rich chains segregation toward the surface. Nonetheless, morphological rearrangement by annealing may rearrange the copolymer chains distribution, Figure 6. Nonetheless, chain rearrangement was restricted in XSAN25 due to its cross-linking. Enhanced glass transition to 120 °C was assigned as the rigid character of SNPs during isothermal crystallization of iPP [41]. The epitaxial β nucleation efficiency also increased by excessive chain entanglements at soft interface rather than precipitation over a rigid substrate [39].

Conclusions

The addition of SAN25-500, XPS, PS400 or XSAN25 soft nanoparticles to iPP caused β modification upraise to 34, 27, 20 and 10%, respectively. Ten minutes isothermal annealing at 116 °C maximized the relative percentage of β modification of all iPP containing SNPs. Annealing time or temperature change declined the relative percentage of β-polymorph of iPP/SAN25-500,

iPP/PS400 and iPP/XSAN25. SAN cross linking forbade SNP's dimensional evolution reducing its β nucleation efficiency to 18 percent. The β nucleation efficiency difference regarding SNPs was attributed to their structural rigidity at crystallization temperature, average phenyl group accessibility for van der Waals interaction with methyl groups of iPP and their relative commensuration mismatch. High efficiency of SAN25-500 was attributed to its phenyl group d-spacing decrease with respect to PS400 and space consistency with β-polymorphism. Finally, stacked phenyl rings and their surface abundance due to cross-linking or co-monomer concentration fluctuation and state of nucleating agent during crystallization of iPP were the most effective parameters leading to β nucleation efficiency.

References:

1 J. Kang, G. Weng, Z. Chen, J. Chen, Y. Cao, F. Yang and M. Xiang, *RSC Adv.*, 2014, **4**, 29514-29526.

2 Y. Wang, C. Chen, J. Xu, J. Lei, Y. Mao, Z. Li and B. S. Hsiao, *J. Phys. Chem. B*, 2012, **116**, 5056–5063.

3 J. Chen, K. Schneider, B. Kretzschmar and G. Heinrich, *Polymer.*, 2014, **55**, 5477–5487.

4 G. T. Offord, S. R. Armstrong, B. D. Freeman, E. Baer, A. Hiltner, J. S. Swinnea and D. R. Paul, *Polymer.*, 2013, **54**, 2577–2589.

5 G. T. Offord, S. R. Armstrong, B. D. Freeman, E. Baer, A. Hiltner and D. R. Paul, *Polymer.*, 2013, **54**, 2796–2807.

6 Z. Su, M. Dong, Z. Guo and J. Yu, *Macromolecules*, 2007, **40**, 4217–4224.

7 S. V. Meille, D. R. Ferro, S. Brückner, A. J. Lovinger and F. J. Padden, *Macromolecules*, 1994, **27**, 2615–2622.

8 F. Luo, C. Geng, K. Wang, H. Deng, F. Chen, Q. Fu and B. Na, *Macromolecules*, 2009, **42**, 9325–9331.

9 Y. H. Chen, G. Zhong, Y. Wang, Z.-M. Li and L. Li, *Macromolecules*, 2009, **42**, 4343–4348.

10 J. Varga, *J. Macromol. Sci. Part B*, 2002, **41**, 1121–1171.

11 R. Lv, Z. Li, B. Na, S. Zou and H. Pan, *J. Appl. Polym. Sci.*, 2012, **125**, 2764–2770.

12 A. Phillips, P. W. Zhu and G. Edward, *Polymer.*, 2010, **51**, 1599–1607.

13 S. Borysiak, *Polym. Eng. Sci.*, 2011, **51**, 2505–2516.

14 W. Wang, M. Fu and B. Qu, *Polym. Adv. Technol.*, 2004, **15**, 467–471.

15 W. Stocker, M. Schumacher, S. Graff, A. Thierry, J. Wittmann and B. Lotz, *Macromolecules*, 1998, **31**, 807–814.

16 H. Li and S. Yan, *Macromolecules*, 2011, **44**, 417–428.

17 K. Cho, D. Kim and S. Yoon, *Macromolecules*, 2003, **36**, 7652–7660.

18 L. Li, C. C. Y. Li and C. Ni, *J. Am. Chem. Soc.*, 2006, **128**, 1692–1699.

19 J. J. P. Yang, Q. Liao, J. J. J. Zhou, X. Jiang, X. H. Wang, Y. Zhang, S. D. Jiang, S. K. Yan and L. Li, *Macromolecules*, 2011, **44**, 3511–3516.

20 A. Tuteja, M. E. Mackay, C. J. Hawker, B. VAN Horn, D. L. Ho and B. Van Horn, *J. Polym. Sci. Part B Polym. Phys.*, 2006, **44**, 1930–1947.

21 T. C. Clancy, J. H. Jang, A. Dhinojwala and W. L. Mattice, *J. Phys. Chem. B*, 2001, **105**, 11493–11497.

22 K. S. Gautam, A. A. D. Schwab, A. Dhinojwala, D. Zhang, S. M. Dougal and M. S. Yeganeh, *Phys. Rev. Lett.*, 2000, **85**, 3854.

23 X. Li, H. Wu, T. Huang, Y. Shi, Y. Wang, F. Xiang and Z. Zhou, *Colloid Polym. Sci.*, 2010, **288**, 1539–1549.

24 H. Mohammadi and N. Mohammadi, *Polymer.*, 2012, **53**, 2769–2776.

25 J. Brandrup, E. Immergut, E. Grulke, A. Abe and D. Bloch, *Polymer handbook*, Wiely-interscience Publication, Inc., 4th ed., 1999.

26 R. Krishnamoorti, W. W. Graessley, G. T. Dee, D. J. Walsh, L. J. Fetters and D. J. Lohse, *Macromolecules*, 1996, **29**, 367–376.

27 A. A. V. G. Ruzette and A. M. A. Mayes, *Macromolecules*, 2001, **34**, 1894–1907.

28 K. Nakamura, S. Shimizu, S. Umemoto, A. Thierry, B. Lotz and N. Okui, *Polym. J.*, 2008, **40**, 915–922.

29 J. Tian, W. Yu and C. Zhou, *J. Macromol. Sci. Part B Phys.*, 2006, **45**, 969–985.

30 H. Bai, F. Luo, T. Zhou, H. Deng, K. Wang and Q. Fu, *Polymer.*, 2011, **52**, 2351–2360.

31 A. Menyhárd, J. Varga and G. Molnár, *J. Therm. Anal. Calorim.*, 2006, **83**, 625–630.

32 B. G. Colvin and P. Storr, *Eur. Polym. J.*, 1974, **10**, 337–340.

33 X. Li, K. Hu, M. Ji, Y. Huang and G. Zhou, *J. Appl. Polym. Sci.*, 2002, **86**, 633–638.

34 S. Mishra and A. Chatterjee, *Polym. Adv. Technol.*, 2011, **22**, 1593–1601.

35 Y. N. Lichao Yin, Jiulin Wang, Fengjiao Lin, Jun Yang, L. Yin, J. Wang, F. Lin, J. Yang and Y. Nuli, *Energy Environ. Sci.*, 2012, **5**, 6966–6972.

36 G. R. Mitchell and A. H. Windle, *Polymer.*, 1984, **25**, 906–920.

37 S. Krimm, *J. Phys. Chem.*, 1953, **57**, 22–25.

38 S. M. Wecker, T. Davidson and J. B. Cohen, *J. Mater. Sci.*, 1972, **7**, 1249–1259.

39 B. Yurdumakan, K. Nanjundiah and A. Dhinojwala, *J. Phys. Chem. C*, 2007, **111**, 960–965.

40 K. K. A. Briggman, J. C. Stephenson, W. E. Wallace and L. J. Richter, *J. Phys. Chem. B*, 2001, **105**, 2785–2791.

41 J. H. Glans and D. T. Turner, *Polymer.*, 1981, **22**, 1540–1543.